

A nonlinear Schrödinger equation for gravity waves slowly modulated by linear shear flow

Shaofeng Li(李少峰), Juan Chen(陈娟), Anzhou Cao(曹安州), Jinbao Song(宋金宝)
Citation: Chin. Phys. B . 2019, 28(12): 124701 . **doi:** 10.1088/1674-1056/ab53cf
Journal homepage: http://cpb.iphy.ac.cn; http://iopscience.iop.org/cpb

What follows is a list of articles you may be interested in

Simulation of a torrential rainstorm in Xinjiang and gravity wave analysis

Rui Yang(杨瑞), Yi Liu(刘毅), Ling-Kun Ran(冉令坤), Yu-Li Zhang(张玉李)
Chin. Phys. B . 2018, 27(5): 059201 . **doi:** 10.1088/1674-1056/27/5/059201

Characteristics and generation of elastic turbulence in a three-dimensional parallel plate channel using direct numerical simulation

Hong-Na Zhang(张红娜), Feng-Chen Li(李凤臣), Xiao-Bin Li(李小斌), Dong-Yang Li(李东阳), Wei-Hua Cai(蔡伟华), Bo Yu(宇波)
Chin. Phys. B . 2016, 25(9): 094701 . **doi:** 10.1088/1674-1056/25/9/094701

Effect of oceanic current on typhoon-wave modeling in the East China Sea

Cui Hong, He Hai-Lun, Liu Xiao-Hui, Li Yi
Chin. Phys. B . 2012, 21(10): 109201 . **doi:** 10.1088/1674-1056/21/10/109201

A nonlinear Schrödinger equation for gravity waves slowly modulated by linear shear flow*

Shaofeng Li(李少峰), Juan Chen(陈娟), Anzhou Cao(曹安州)†, and Jinbao Song(宋金宝)‡

Ocean College, Zhejiang University, Zhoushan 316000, *China*

(Received 9 September 2019; revised manuscript received 18 October 2019; published online 29 November 2019)

Assume that a fluid is inviscid, incompressible, and irrotational. A nonlinear Schrödinger equation (NLSE) describing the evolution of gravity waves in finite water depth is derived using the multiple-scale analysis method. The gravity waves are influenced by a linear shear flow, which is composed of a uniform flow and a shear flow with constant vorticity. The modulational instability (MI) of the NLSE is analyzed, and the region of the MI for gravity waves (the necessary condition for existence of freak waves) is identified. In this work, the uniform background flows along or against wave propagation are referred to as down-flow and up-flow, respectively. Uniform up-flow enhances the MI, whereas uniform down-flow reduces it. Positive vorticity enhances the MI, while negative vorticity reduces it. Hence, the influence of positive (negative) vorticity on MI can be balanced out by that of uniform down (up) flow. Furthermore, the Peregrine breather solution of the NLSE is applied to freak waves. Uniform up-flow increases the steepness of the free surface elevation, while uniform down-flow decreases it. Positive vorticity increases the steepness of the free surface elevation, whereas negative vorticity decreases it.

Keywords: nonlinear Schrödinger equation, gravity waves, linear shear flow, modulational instability

PACS: 92.10.Hm, 47.35.Bb, 47.35.De **DOI:** 10.1088/1674-1056/ab53cf

1. Introduction

Wave phenomena including freak waves, internal waves, tsunamis, tides, and storm surges are abundant in oceans. Generation and evolution of these waves with different scales are usually related to combination of gravity, rotation of the earth, buoyancy, and gravitation of the moon and the sun. In this study, we focus on the surface gravity waves, of which the restoring force is gravity. Here the uniform flows along or against wave propagation are referred to as down-flow and up-flow, respectively. Using the multiple-scale analysis method, Davey and Stewartson[1] for the first time derived the nonlinear Schrödinger equation (NLSE) which describes the evolution of three-dimensional wave trains in a finite water depth. They also analyzed the instability of surface gravity waves due to small disturbances. Turpin *et al.*[2] further found that the amplitude of surface gravity waves meets the cubic NLSE. They evaluated the hypothesis of Djordjevic and Redelopp,[3] and showed that the evolution of surface gravity waves is directly connected to the instability parameter, which depends on depth and current variation. The evolution of surface gravity waves with current has been explored in many previous studies, such as Peregrine,[4] Longuet-Higgins and Stewart,[5] and Kantardgi.[6] Moreover, Maciver *et al.*[7] evaluated the kinematics and dynamics of the interaction of waves and currents through laboratory experiments. They found that down-flow increases wavelength and reduces wave height, whereas up-flow has the opposite influence. Based on a numerical method, Choi[8] also found that the maximal wave amplitude with down-flow is much smaller than that with no flow, whereas up-flow produces the opposite result. Ma *et al.*[9] indicated that up-flow can block the wave energy and destroy the conservation of wave action in a flume, which boosts the asymmetric modulation. Ma *et al.*[1] further showed that up-flow can speed up the growth of modulational instability (MI), qualitatively verifying their previous theory.[9] In addition, Sedletsky[11] studied the MI of wave trains and displayed the limit $kh = 1.363$. Toffoli *et al.*[12] assessed the effect of up-flow on changing the statistical properties of wave fields through experiments. Especially, Thomas *et al.*[13] analyzed the effects of the vorticity on the instability properties of nonlinear wave trains. They pointed out that the vorticity effectively modifies the MI of gravity waves. As a special kind of surface waves, freak waves can also be described by the NSLE. Smith[14] showed that freak waves can be created by strong up-flow. Henderson *et al.*[15] further proposed some breather solutions of the NLSE for freak waves. Dysthe and Trulsen[16] strengthened the solution proposed by Henderson *et al.*[15] by comparing it with the simulation data. Among the breather solutions,[15,16] the Ma breather solution[17] and Peregrine breather (PB) solution[18] are very useful for freak waves. Tao *et al.*[19] constructed rogue wave solutions using the Darboux transformation of the NLSE, and revealed that the desired shape of freak waves can be generated by suitably adjusting the physical parameters. Kharif and Pelinovsky[20]

*Project supported by the National Key Research and Development Program of China (Grant Nos. 2016YFC1401404 and 2017YFA0604102) and the National Natural Science Foundation of China (Grant No. 41830533).

†Corresponding author. E-mail: caoanzhou@zju.edu.cn

‡Corresponding author. E-mail: songjb@zju.edu.cn

© 2019 Chinese Physical Society and IOP Publishing Ltd

showed the main physical mechanisms of freak waves by combining numerical simulations performed in the framework of the Korteweg–de Vries (KdV) equation and the NLSE, together with the analysis of data from marine observations and laboratory experiments. Recently, Liao *et al.*[21] studied the MI of the NLSE and freak waves with linear shear flow, and found that the effect of vorticity can balance the influence of uniform flow on instability and freak waves.

In coastal zones, the propagation of gravity waves is principally affected by the flow and bathymetry variation. Touboul *et al.*[22] demonstrated the influence of horizontal vorticity associated with the background current profile on the propagation of waves in coastal areas. In a realistic ocean, neglecting the vertical structure of currents may lead to significant errors in wave amplitude, and an account of the vertical shear may be better coupled to modern circulation models.[23] However, the realistic case is somewhat complicated. To better understand the mechanism by which the background current and vorticity has an influence on gravity waves, it is necessary to theoretically explore a simplified case.

This study is an extension of Thomas *et al.*[13] Based on the multiple-scale analysis method, the NLSE for gravity waves with linear shear flow is derived in Section 2. The MI of gravity waves is analyzed in Section 3. Based on the PB solution, the effect of linear shear flow on freak waves is explored in Section 4. Finally, the conclusions of this study are presented in Section 5.

2. Mathematical methods

Assume that a fluid is inviscid, incompressible, and irrotational, and consider a case in which two-dimensional gravity waves propagate in a finite water depth, with the existence of a linear shear flow. A fully Eulerian frame ($oxyz$) with unit vectors ($\boldsymbol{i}$, $\boldsymbol{j}$, $\boldsymbol{k}$) is used, as shown in Fig. 1. In the figure, the x axis points to the direction of propagation of the wave trains, the y axis points upward, and the z axis points straight out of the page. Therefore, the gravitational acceleration is $\boldsymbol{g}=-g\boldsymbol{j}$ with $g>0$. Here the uniform background flows along or against the direction of wave propagation are referred to as down-flow and up-flow, respectively.

Thereafter, the total fluid velocity can be written as

$$\boldsymbol{V}=(U+\Omega y)\boldsymbol{i}+\nabla\phi(x,y,t), \tag{1}$$

where a constant U represents the uniform flow in the water column, a constant Ω is the vorticity and denotes the magnitude of the linear shear, $\nabla\phi(x,y,t)$ is the wave induced velocity, $\nabla=(\partial/\partial x,\partial/\partial y)$ is the two-dimensional gradient operator, ϕ is the velocity potential function, and t is time. Without loss of generality, it is assumed that the waves propagate along the positive x axis. The governing equations[21,24,25] for the waves are displayed as follows:

$$\begin{aligned}
&\Delta\phi=0, \quad -h<y<\zeta(x,t);\\
&\phi_y=0, \quad y=-h;\\
&\zeta_t+(\phi_x+U+\Omega\zeta)\zeta_x-\phi_y=0, \quad y=\zeta;\\
&\phi_{tx}+\phi_{ty}\zeta_x+(\phi_x+U+\Omega\zeta)(\phi_{xx}+\phi_{xy}\zeta_x)\\
&+\phi_y(\phi_{xy}+\phi_{yy}\zeta_x)+\Omega\phi_y+g\zeta_x=0, \quad y=\zeta,
\end{aligned} \tag{2}$$

where h is a constant and denotes the flat bottom ($y=-h$) and $\zeta(x,t)$ is the free surface elevation. The subscript stands for derivatives of the corresponding variable.

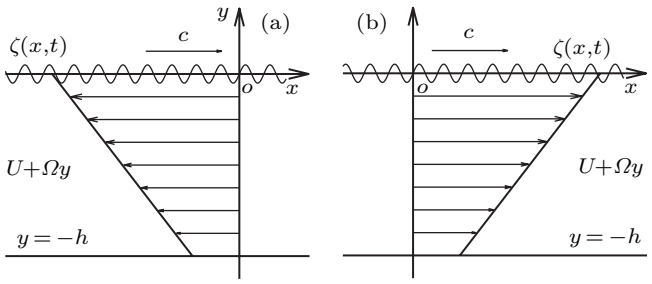


Fig. 1. Schematic of the Eulerian framework for two-dimensional propagating gravity waves with a linear shear flow. Here $\zeta(x,t)$ is the free surface elevation and c is the wave velocity. (a) Waves propagating upstream with uniform up-flow ($U<0$) and negative vorticity ($\Omega<0$). (b) Waves propagating downstream with uniform down-flow ($U>0$) and positive vorticity ($\Omega>0$).

2.1. The multiple scale stretching transforms

The higher harmonic term is produced by the nonlinear term, which impacts on the original harmonic and makes the amplitude of waves change slowly with space and time. Following Davey and Stewartson,[1] the multiple scale method is adopted to derive the evolution equation

$$\eta=\varepsilon(x-c_{\mathrm{g}}t), \quad \tau=\varepsilon^2 t, \tag{3}$$

where $\varepsilon=kA$ is a small parameter characterizing the steepness of the wave trains, η and τ are the slower variables in space and time, k, A, and c_{g} are the wave number, amplitude, and group velocity of the carrier wave in the presence of linear shear flow, respectively. Therefore, the governing equations become

$$\begin{aligned}
&\varepsilon^2\phi_{\eta\eta}+\phi_{yy}=0, \quad -h<y<\zeta(\eta,\tau); \quad \phi_y=0, \quad y=-h;\\
&\varepsilon^2\zeta_\tau-\varepsilon c_{\mathrm{g}}\zeta_\eta+\varepsilon\zeta_\eta(\varepsilon\phi_\eta+U+\Omega\zeta)-\phi_y=0, \quad y=\zeta;\\
&\varepsilon^3\phi_{\eta\tau}-\varepsilon^2 c_{\mathrm{g}}\phi_{\eta\eta}+\varepsilon^3\phi_{y\tau}\zeta_\eta-\varepsilon^2 c_{\mathrm{g}}\phi_{\eta y}\zeta_\eta\\
&+\varepsilon\phi_y(\phi_{\eta y}+\phi_{yy}\zeta_\eta)+(\varepsilon^3\phi_\eta+\varepsilon^2 U+\varepsilon^2\Omega\zeta)\\
&\times(\phi_{\eta\eta}+\phi_{\eta y}\zeta_\eta)+\Omega\phi_y+\varepsilon g\zeta_\eta=0, \quad y=\zeta.
\end{aligned} \tag{4}$$

Note that equation (4) matches the result of Thomas *et al.*[13] when $U=0$.

2.2. Derivation of the NLSE with linear shear flow

The velocity potential ϕ is expanded in a Taylor series of ζ about the horizontal line ($y=0$) and substituted into the upper boundary conditions of Eq. (4). Then an asymptotic solution to equation (4) is assumed in the form:

$$\phi=\sum_{n=-\infty}^{+\infty}\phi_n\exp\left[\mathrm{i}n(kx-\omega t)\right],$$

$$\zeta = \sum_{n=-\infty}^{+\infty} \zeta_n \exp\left[\mathrm{i}n\left(kx-\omega t\right)\right]. \tag{5}$$

Here ω is the angular frequency and n is the order of harmonics. We set $\phi_{-n}=\phi_n^*$ and $\zeta_{-n}=\zeta_n^*$, where the asterisk denotes the complex conjugate. The ϕ_n and ζ_n are expanded in a perturbation series of ε:

$$\phi_n = \sum_{m=n}^{+\infty} \varepsilon^m \phi_{nm}(\eta, y, \tau), \quad \zeta_n = \sum_{m=n}^{+\infty} \varepsilon^m \zeta_{nm}(\eta, \tau), \tag{6}$$

where m is the order and $\phi_{00}=\zeta_{00}=0$ is assumed. Substituting Eqs. (5) and (6) into Eq. (4), and separating the different orders and harmonics, a set of ordinary linear differential equations for ϕ_{nm} and ζ_{nm} is obtained. The detailed expressions are given in Appendix. After somewhat tedious derivation, the NLSE of linear shear flow for envelope A is obtained as follows:

$$\mathrm{i}\frac{\partial A}{\partial \tau} + \alpha \frac{\partial^2 A}{\partial \eta^2} = \beta |A|^2 A, \tag{7}$$

$$\alpha = \frac{\omega}{k^2\sigma\left(2+X-2\bar{u}\right)}\left\{\mu\left(1-\sigma^2\right)\left[\left(1-\mu\sigma\right)\left(1-\bar{u}\right)^2 + \left(1-\bar{c}_{\mathrm{g}}\right)X\right] - \sigma\left(\bar{c}_{\mathrm{g}}-\bar{u}\right)^2\right\}, \tag{8}$$

$$\beta = \frac{k^3\omega\left(MG+H\right)}{2g\sigma^3\left(2+X-2\bar{u}\right)}, \tag{9}$$

$$M = \left(\sigma\bar{c}_{\mathrm{g}} - \sigma\bar{u} + \mu X\right)\left[\left(1+X-\bar{u}\right)^2 - \sigma^2\left(1-\bar{u}\right)^2\right] + \sigma\left(1-\bar{u}\right)\left(1+X-\bar{u}\right)\left(2+X-2\bar{u}\right), \tag{10}$$

$$G = 2\sigma^2 \frac{\left(1+X-\bar{u}\right)\left(2+X-2\bar{u}\right) + \left(1-\sigma^2\right)\left(\bar{c}_{\mathrm{g}}-\bar{u}\right)\left(1-\bar{u}\right)}{\left(1-\bar{u}\right)\left[\left(\bar{c}_{\mathrm{g}}-\bar{u}\right)\left(\sigma\bar{c}_{\mathrm{g}}-\sigma\bar{u}+\mu X\right) - \mu\left(1+X-\bar{u}\right)\left(1-\bar{u}\right)\right]}, \tag{11}$$

$$H = \left(-2\sigma^6+13\sigma^4-12\sigma^2+9\right)\left(1-\bar{u}\right)^2 + \left(15\sigma^4-18\sigma^2+27\right)\left(1-\bar{u}\right)X + \left(4\sigma^4-3\sigma^2+33\right)X^2 + \left(5\sigma^2+21\right)\left(1-\bar{u}\right)^{-1}X^3 + \left(2\sigma^2+7\right)\left(1-\bar{u}\right)^{-2}X^4 + \left(1-\bar{u}\right)^{-3}X^5, \tag{12}$$

where $\bar{c}_{\mathrm{g}} = c_{\mathrm{g}}/c$ is the dimensionless group velocity, and α and β are the dissipation and nonlinear coefficients, which depend on ($\bar{u}$, X, μ). If $\bar{u}=0$, then equations (7)–(12) are the same as those derived by Thomas *et al.*[13] Equation (11) displays the coupling between the mean flow and the linear shear flow. We also obtain the equation of free surface for the envelope B

$$\zeta = \frac{1}{2}\left(\varepsilon B \mathrm{e}^{\mathrm{i}(kx-\omega t)} + \varepsilon B^* \mathrm{e}^{-\mathrm{i}(kx-\omega t)}\right) + O(\varepsilon^2), \tag{13}$$

$$\mathrm{i}\frac{\partial B}{\partial \tau} + \alpha \frac{\partial^2 B}{\partial \eta^2} = \gamma |B|^2 B, \ \gamma = \frac{\omega^2\left(1-\bar{u}\right)^2}{4k^2\sigma^2}\beta. \tag{14}$$

We also need to study the case of an infinite depth. When $\mu \to \infty$, the NLSE with linear shear flow and infinite water depth becomes

$$\mathrm{i}\frac{\partial B}{\partial \tau} - \frac{\omega}{k^2}\frac{\left(1+\bar{\Omega}-\bar{u}\right)^2\left(1-\bar{u}\right)^2}{\left(2+\overline{\Omega}-2\bar{u}\right)^3}\frac{\partial^2 B}{\partial \eta^2} = \frac{k^2\omega}{8\left(1+\bar{\Omega}-\bar{u}\right)\left(1-\bar{u}\right)}\left[4\left(1-\bar{u}\right)^3 + 10\left(1-\bar{u}\right)^2\bar{\Omega} + 8\left(1-\bar{u}\right)\bar{\Omega}^2 + 3\bar{\Omega}^3\right]|B|^2 B. \tag{15}$$

In the system, the wave trains can travel both downstream and upstream if $|U|<c$. When $|U|<c$, $|U|=c$, and $|U|>c$, the flow is subcritical, critical, and supercritical, respectively. In this study, we only consider the subcritical flow with $-1<\bar{u}<1$. Hence, according to the dispersion relation (Appendix), it is easy to find $X>\bar{u}-1$. In an infinite depth, $\sigma=1$, $\bar{\Omega}=X>\bar{u}-1$. According to Eq. (15), $\bar{\Omega}$ has two zeros $\bar{u}-1$ and $\frac{2}{3}\bar{u}-\frac{2}{3}$ and two singularities $2\bar{u}-2$ and $\bar{u}-1$, respectively. Given that $\bar{u}-1$, $2\bar{u}-2$ must not be larger than $\bar{u}-1$. Therefore, $\bar{\Omega}$ cannot be equal to $\bar{u}-1$ or $2\bar{u}-2$. If $\bar{\Omega}$ is equal to $\frac{2}{3}\bar{u}-\frac{2}{3}$, the nonlinear coefficient becomes zero and the NLSE is reduced to the Schrödinger equation

$$\mathrm{i}\frac{\partial B}{\partial \tau} - \frac{3}{64}\frac{\omega}{k^2}\left(1-\bar{u}\right)\frac{\partial^2 B}{\partial \eta^2} = 0,$$

or

$$\mathrm{i}\frac{\partial B}{\partial \tau} + \frac{9}{128}\frac{\omega}{k^2}\bar{\Omega}\frac{\partial^2 B}{\partial \eta^2} = 0. \tag{16}$$

3. MI analysis

It has been widely known that MI analysis can present us an approximate characterization on the stability of perturbations.[26,27] Note that in the case of $\alpha\gamma<0$ corresponding to the focusing nonlinear equation, it admits MI and modulational stability (MS) regime on the MI gain spectrum distribution. However, in the case of $\alpha\gamma>0$ corresponding to the defocusing nonlinear equation, it admits no MI regime.[28,29] The dispersion relation for perturbation can be given as follows:[13]

$$\Gamma^2 = \alpha L^2\left(\alpha L^2 + 2\gamma B_0^2\right), \tag{17}$$

where B_0 is initial amplitude, L and Γ are the perturbations in wave number and angular frequency, respectively. The growth rate of MI is given by

$$\Gamma_{\mathrm{i}} = L\sqrt{-2\alpha\gamma B_0^2 - \alpha^2 L^2}. \tag{18}$$

The dimensionless growth rate of MI is

$$\bar{\Gamma}_{\mathrm{i}} = \bar{L}\sqrt{-2\bar{\alpha}\bar{\gamma} - \bar{\alpha}^2\bar{L}^2}, \tag{19}$$

where

$$\bar{\alpha}=\frac{k^2}{\omega}\alpha,\quad \bar{\gamma}=\frac{\gamma}{\omega k^2},\quad \bar{L}=\frac{L}{B_0k^2},\quad \bar{\Gamma_{\rm i}}=\frac{\Gamma_{\rm i}}{\omega B_0^2k^2} \tag{20}$$

are the dimensionless variables, which only depend on $(\bar{u},X,\mu)$. According to Eq. (19), when

$$\bar{L}=\sqrt{-\frac{\bar{\gamma}}{\bar{\alpha}}}, \tag{21}$$

the dimensionless growth rate reaches a maximum

$$\bar{\Gamma_{\rm i}}_{\max}=\sqrt{-\frac{\bar{\gamma}}{\bar{\alpha}}}\sqrt{-\bar{\alpha}\bar{\gamma}}=|\bar{\gamma}|. \tag{22}$$

Thereafter, the dimensionless bandwidth of instability is obtained

$$\Lambda\bar{L}=\sqrt{2}\bar{L}=\sqrt{-2\frac{\bar{\gamma}}{\bar{\alpha}}}. \tag{23}$$

Figure 2 displays the stable and unstable regions of gravity wave trains in the (X,μ) space for $\bar{u}$ varying from -0.9 to 0.9, with an interval of 0.3. For each $\bar{u}$, the curve $\alpha\gamma=0$ divides the (X,μ) space into stable and unstable regions. When $\bar{u}=0$, the curve $\alpha\gamma=0$ has the asymptote $X=-2/3$, which is consistent with the result of Thomas *et al.*[13] The MS occurs in the interval $\bar{u}-1<X\leq\frac{2}{3}\bar{u}-\frac{2}{3}$, which is equivalent to $-\infty<\Omega\leq-2(gk/3\sigma)^{1/2}$. When $2/3\bar{u}-2/3<X<+\infty$ $[-2(gk/3\sigma)^{1/2}<\Omega<+\infty]$, the wave train is unstable above the curve $\alpha\gamma=0$, whereas it is stable below the curve. Furthermore, the curve $\alpha\gamma=0$ for each $\bar{u}$ has a node at the critical value $\mu=1.363$, which is consistent with Sedletsky.[11] Without the shear, the wave train is stable if μ is smaller than the critical value of 1.363. Otherwise, the wave train is unstable. In addition, it is found that with the increase of $\bar{u}$, the asymptote of the curve $\alpha\gamma=0$ moves to the right and the unstable region becomes smaller.

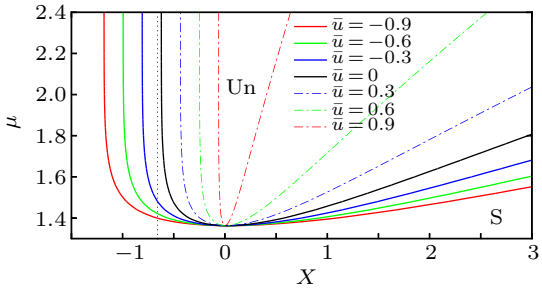


Fig. 2. The (X,μ)-stability diagram for gravity waves. S and Un denote the stable and unstable regions for each value of $\bar{u}$. The black dotted line denotes $X=-2/3$.

In the case of infinite depth, according to Eq. (15) we have

$$\begin{aligned}\alpha\gamma=&-\frac{\omega^2}{8}(1-\bar{u})\left(1+\bar{\Omega}-\bar{u}\right)\left[3\bar{\Omega}+2(1-\bar{u})\right]\\&\times\left[\bar{\Omega}^2+2(1-\bar{u})\bar{\Omega}+2(1-\bar{u})^2\right]\\&\times\left(2+\bar{\Omega}-2\bar{u}\right)^{-3}.\end{aligned} \tag{24}$$

The gravity waves are stable when $-\infty<\Omega\leq-2(gk/3)^{1/2}$, while they are unstable when $-2(gk/3)^{1/2}<\Omega<+\infty$.

The growth rate of MI $\Gamma_{\rm i}$ on B_0 and L is demonstrated in Fig. 3. It shows that the white asymptote divides the (B_0, L) space into MI and MS regions. We can qualitatively see that in MI regions the small perturbations are unstable and can be amplified exponentially. In MS regions the ones are stable and do not grow up. Without the consideration of linear shear flow, figure 3(b) is same as the one of Zhao *et al.*[26]

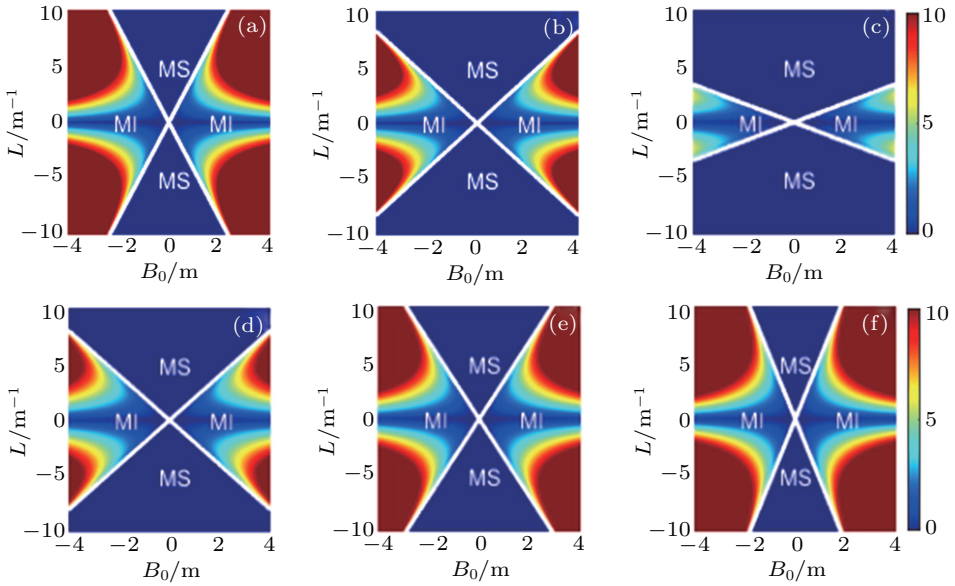


Fig. 3. The MI gain spectrum $\Gamma_{\rm i}$ distributed on the initial amplitude and perturbation wave number space for $\omega=3.4$ Hz: (a) $\mu=2$, $\bar{\Omega}=0$, $\bar{u}=-0.2$; (b) $\mu=2$, $\bar{\Omega}=0$, $\bar{u}=0$; (c) $\mu=2$, $\bar{\Omega}=0$, $\bar{u}=0.2$; (d) $\mu=5$, $\bar{u}=0$, $\bar{\Omega}=-0.2$; (e) $\mu=5$, $\bar{u}=0$, $\bar{\Omega}=0$; (f) $\mu=5$, $\bar{u}=0$, $\bar{\Omega}=0.2$. MI and MS denote modulational instability and modulational stability, respectively.

From Figs. 3(a)–3(c), it is seen that uniform up-flow increases the MI region whereas uniform down-flow decreases it. From Figs. 3(d)–3(f), it is seen that negative vorticity decreases the MI region whereas positive vorticity increases it. The MI region becomes larger with the increase of water depth as shown in Figs. 3(b) and 3(e).

3.1. The maximum dimensionless growth rate of instability

Figure 4 presents the ratio of $\overline{\Gamma}_{\mathrm{i\,max}}$ over $\overline{\Gamma}_{\mathrm{i\,max0}}$ for the maximum dimensionless growth rate of MI influenced by the dimensionless water depth μ, uniform flow $\bar{u}$, and vorticity $\bar{\Omega}$. The ratio increases at first and then decreases with the increase of $\bar{\Omega}$ in a finite depth, whereas it always increases with the increase of $\bar{\Omega}$ in an infinite depth. In addition, a larger μ would cause a larger range of $\bar{\Omega}$, i.e., the corresponding gravity waves have a larger unstable region. The unstable region would become broader with the decrease of $\bar{u}$.

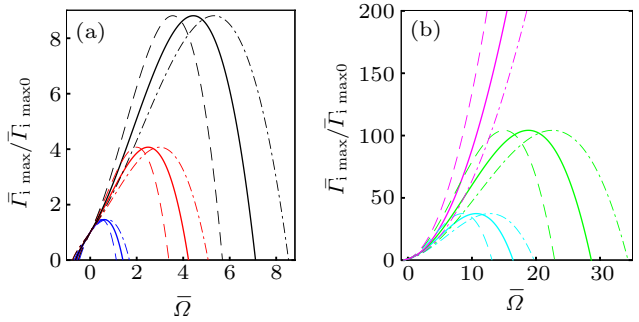


Fig. 4. The ratio of $\overline{\Gamma}_{\mathrm{i\,max}}$ over $\overline{\Gamma}_{\mathrm{i\,max0}}$ as a function of $\bar{\Omega}$ for $\bar{u}=-0.2$ (dot-dashed line), $\bar{u}=0$ (solid line), $\bar{u}=0.2$ (dashed line): (a) $\mu=1.5$ (blue), $\mu=2$ (red), and $\mu=2.5$ (black); (b) $\mu=4$ (cyan), $\mu=6$ (green) and $\mu=+\infty$ (magenta). $\overline{\Gamma}_{\mathrm{i\,max0}}$ is the maximum dimensionless growth rate for $\bar{\Omega}=0$.

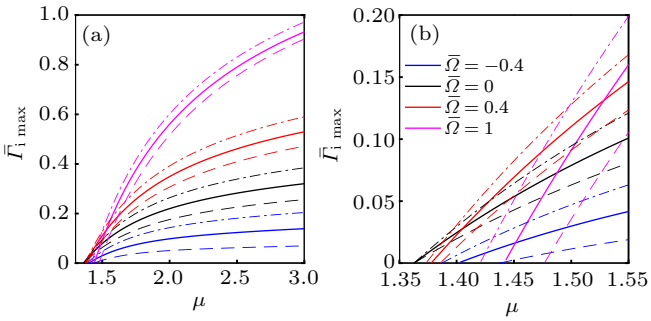


Fig. 5. $\overline{\Gamma}_{\mathrm{i\,max}}$ as a function of μ for $\bar{u}=-0.2$ (dot-dashed line), $\bar{u}=0$ (solid line), $\bar{u}=0.2$ (dashed line): (a) $\bar{\Omega}=-0.4$ (blue), $\bar{\Omega}=0$ (black), $\bar{\Omega}=0.4$ (red), $\bar{\Omega}=1$ (magenta); (b) part of (a) for $1.35<\mu\leq 1.55$.

Figure 5 shows the maximum dimensionless growth rate $\overline{\Gamma}_{\mathrm{i\,max}}$ as a function of dimensionless water depth μ for different $\bar{u}$ and $\bar{\Omega}$. It can be clearly seen that $\overline{\Gamma}_{\mathrm{i\,max}}$ displays an increasing trend with μ. Compared with the case without vorticity, a positive vorticity enhances $\overline{\Gamma}_{\mathrm{i\,max}}$, while a negative vorticity reduces it. Moreover, uniform down-flow decreases $\overline{\Gamma}_{\mathrm{i\,max}}$, whereas uniform up-flow increases it. For the case without vorticity, the minimum value of μ is 1.363 regardless of what the uniform flow may be. However, when vorticity exists in the flow, the minimum value of μ would become larger, regardless of whether the vorticity is positive or negative. In addition, with the existence of vorticity, uniform down-flow would increase the minimum value of μ, whereas uniform up-flow would decrease the minimum value of μ.

3.2. The dimensionless growth rate of instability

The dimensionless growth rate $\overline{\Gamma}_{\mathrm{i}}$ as a function of dimensionless perturbation wave number $\bar{L}$ for different μ, $\bar{u}$, and $\bar{\Omega}$ is presented in Fig. 6. Overall, the pattern of the dimensionless growth rate $\overline{\Gamma}_{\mathrm{i}}$ is almost a parabola in both finite and infinite depths. It is clearly shown that a positive vorticity increases $\overline{\Gamma}_{\mathrm{i}}$ and $\Lambda\bar{L}$, whereas a negative vorticity has a reverse effect. Uniform up-flow enhances the MI, whereas uniform down-flow reduces it. For the case without vorticity, the bandwidth $\Lambda\bar{L}$ is the same for different values of $\bar{u}$. However, when the vorticity is negative, uniform up-flow increases $\Lambda\bar{L}$ and uniform down-flow decreases it. In contrast, when the vorticity is positive, uniform up-flow decreases $\Lambda\bar{L}$ and uniform down-flow increases it. In addition, the unstable region will become larger with the increase of μ.

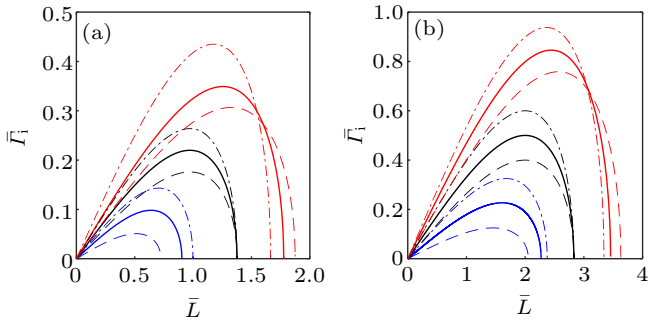


Fig. 6. Dimensionless growth rate as a function of $\bar{L}$ for $\bar{u}=-0.2$ (dot-dashed line), $\bar{u}=0$ (solid line), $\bar{u}=0.2$ (dashed line), $\bar{\Omega}=-0.4$ (blue), $\bar{\Omega}=0$ (black), $\bar{\Omega}=0.4$ (red): (a) $\mu=2$; (b) $\mu=+\infty$.

4. The application

In the following, we apply the NLSE to freak waves, which usually have extraordinarily large wave heights and cause multiple maritime accidents. From rough sea surface, the NLSE models have also been extensively applied to simulate electromagnetic scattering.[30,31] Here the PB,[18] which is one theoretical solution to the NLSE, has become the mainstream method for studying the mechanisms of freak waves. The dimensionless NLSE and its PB solution can be written as

$$\mathrm{i}\frac{\partial\bar{B}}{\partial\bar{\tau}}+\frac{\partial^2\bar{B}}{\partial\bar{\eta}^2}+2|\bar{B}|^2\bar{B}=0, \tag{25}$$

$$\bar{B}(\bar{\eta},\bar{\tau})=\exp(\mathrm{i}2\bar{\tau})\left[\frac{4(1+\mathrm{i}4\bar{\tau})}{1+4\bar{\eta}^2+16\bar{\tau}^2}-1\right], \tag{26}$$

where the bar denotes the normalized coordinate. The formal transformations are taken into consideration:

$$\bar{B}=\frac{B}{B_0},\quad \bar{\tau}=-\frac{\gamma}{2}B_0^2\tau,\quad \bar{\eta}=\sqrt{-\frac{\gamma}{2\alpha}}B_0\eta, \tag{27}$$

with B_0 being the initial amplitude. Substituting the above transform (27) into Eqs. (25) and (26), the dimensionless equation (25) becomes the NLSE (14), and the dimensionless solution (26) leads to the following dimensional solution:

$$B = B_0 \exp\left(-\mathrm{i}\gamma B_0^2 \tau\right) \left[\frac{4\alpha(1-\mathrm{i}2\gamma B_0^2\tau)}{\alpha - 2\gamma B_0^2\eta^2 + \alpha(2\gamma B_0^2\tau)^2} - 1\right]. \quad (28)$$

Figure 7(a) shows the envelope amplitude of carrier waves based on the PB solution. The maximum peak of amplitude is three times larger than the initial value. At the same time, there are two minimum values of zero near the origin. The amplitude of the PB solution is not decreased continuously with the distance from the freak waves. Instead, it tends to be a constant, which reflects the local energy transfer in the evolution of freak waves.

In practical applications, the free surface elevation of freak waves is of great importance. In the first order approximation, the surface elevation of freak waves by adopting Eq. (13) is expressed as follows:

$$\begin{aligned}
&\zeta(x,t) \\
&= \varepsilon B_0 \left\{ \cos(kx - wt) \left[\cos\theta\left(\frac{4\alpha}{\delta} - 1\right) - \sin\theta\frac{8\alpha\theta}{\delta}\right] \right. \\
&\quad \left. + \sin(kx - wt) \left[\sin\theta\left(\frac{4\alpha}{\delta} - 1\right) + \cos\theta\frac{8\alpha\theta}{\delta}\right] \right\}, \quad (29) \\
\theta &= \gamma B_0^2 \varepsilon^2 t, \\
\delta &= \alpha - 2\gamma B_0^2 \varepsilon^2 (x - c_g t)^2 + \alpha(2\gamma B_0^2 \varepsilon^2 t)^2. \quad (30)
\end{aligned}$$

Figure 7(b) shows an example in which the freak waves are assumed to come from negative time. As the figure shows, the free surface elevation is modulated slowly, and the envelope curve has five large crests and four large troughs.

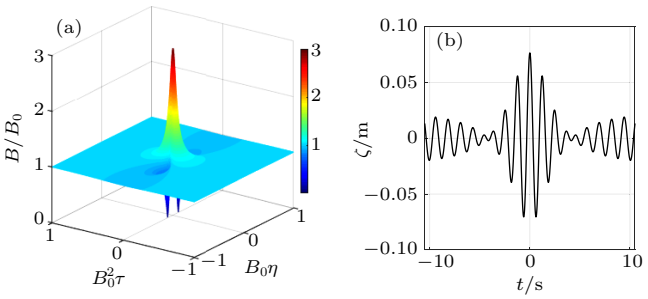


Fig. 7. For $\omega = 5$ Hz, $\mu = 5$. (a) Absolute value of the complex amplitude based on the Peregrine breather (PB) solution. (b) The free surface elevation as a function of time, with $B_0 = 0.1$ m.

Figure 8 shows the free surface elevation as a function of time for different uniform flows, vorticities, and water depths. Given that the waveform (Eq. (29)) is symmetric with respect to time, only the free surface elevation at a positive time is shown. As shown in Figs. 8(a)–8(c), uniform up-flow increases the steepness of free surface elevation, while uniform down-flow decreases it. This is consistent with the aforementioned analysis, which reveals that uniform up-flow enhances the MI but uniform down-flow reduces it. In other words, uniform up-flow decreases the spatiotemporal span of freak waves. This result also indicates that freak waves influenced by uniform up-flow have more concentrated energy and hence more destructive power. Furthermore, the steepness of free surface elevation is decreased by negative vorticity but increased by positive vorticity. The effect of vorticity on the steepness of free surface elevation is opposite to that of uniform flow. In other words, the influence of negative vorticity on the steepness of free surface elevation can be offset by the uniform up-flow, and vice versa. For example, as shown in Fig. 8(d), the blue solid curve ($\bar{u} = 0$, $\bar{\Omega} = -0.2$) is almost coincident with the red dashed curve ($\bar{u} = 0.2$, $\bar{\Omega} = 0.2$), and the red solid curve ($\bar{u} = 0$, $\bar{\Omega} = 0.2$) is almost coincident with the blue dot-dashed curve ($\bar{u} = -0.2$, $\bar{\Omega} = -0.2$). In addition, as shown in Fig. 9, the water depth has a considerable contribution to the free surface elevation of freak waves. The free surface elevation in the shallow water is larger than that in the deep water, suggesting that freak waves are more dangerous in shallow water. This is consistent with Didenkulova *et al.*[32] However, when $\mu > 5$, the influence of water depth can be neglected.[13]

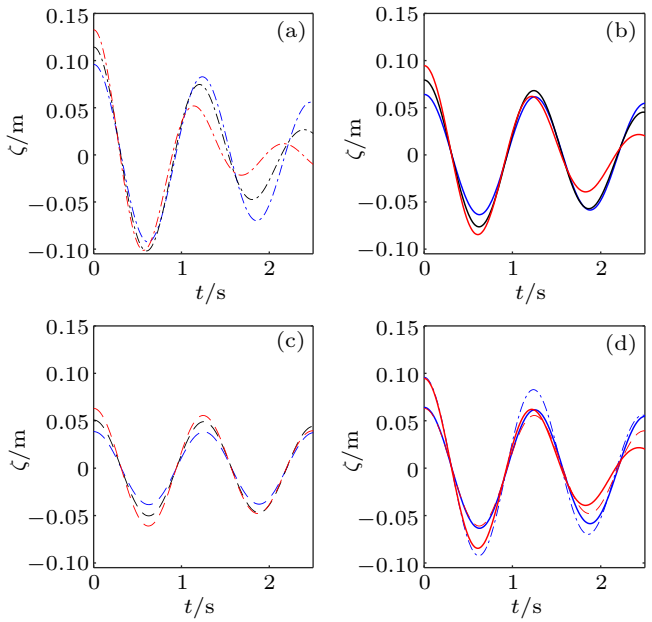


Fig. 8. The free surface elevation as a function of time with $\omega = 5$ Hz, $B_0 = 0.1$ m, $\mu = 2$, $\bar{\Omega} = -0.2$ (blue), $\bar{\Omega} = 0$ (black), and $\bar{\Omega} = 0.2$ (red): (a) $\bar{u} = -0.2$ (dot-dashed line); (b) $\bar{u} = 0$ (solid line); (c) $\bar{u} = 0.2$ (dashed line); (d) the coincidence of the free surface elevation from (a), (b), and (c).

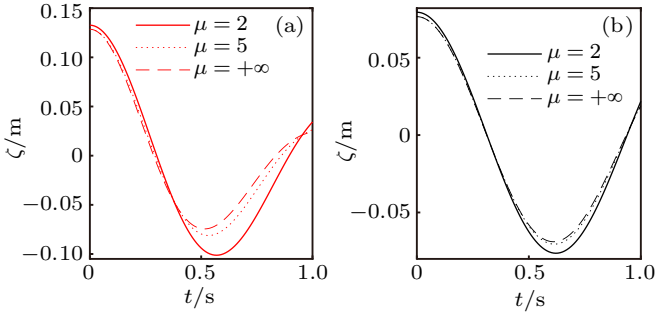


Fig. 9. The free surface elevation as a function of time with $\omega = 5$ Hz, $B_0 = 0.1$ m: (a) $\bar{u} = -0.2$, $\bar{\Omega} = 0.2$; (b) $\bar{u} = 0$, $\bar{\Omega} = 0$.

5. Conclusion

The two-dimensional NLSE describing the evolution of gravity waves in a finite depth with linear shear flow can be derived using the multiple-scale analysis method. By analyzing the MI, it is found that the instability of gravity waves depends on the sign of the product of the dissipation coefficient α and the nonlinear coefficient γ of the NLSE. The stable ($\alpha\gamma>0$) and unstable ($\alpha\gamma<0$) regions in the (X,μ) space for difference cases are displayed. With an increase in uniform flow, the unstable region moves to the right and becomes smaller. The threshold for stable gravity waves in a finite depth is $\Omega=-2(gk/3\sigma)^{1/2}$ and it becomes $\Omega=-2(gk/3)^{1/2}$ in an infinite depth. In addition, the dimensionless growth rate of instability shows an increasing trend with water depth. Uniform up-flow enhances the MI, whereas uniform down-flow reduces it. Positive vorticity enhances the MI, whereas negative vorticity reduces it. In other words, the influence of positive (negative) vorticity on the MI can be balanced out by that of uniform down-flow (up-flow). Moreover, uniform up-flow increases the bandwidth of instability, while uniform down-flow decreases it when vorticity is positive. The influence of uniform flow is opposite to that of negative vorticity.

The PB solution, one theoretical solution of the NLSE, is used to investigate the mechanisms controlling freak waves in this study. It is found that uniform up-flow increases the steepness of the free surface elevation, whereas uniform down-flow decreases it. This result also indicates that freak waves influenced by uniform up-flow have more concentrated energy and hence more destructive power. The steepness is also decreased by negative vorticity, whereas it is increased by positive vorticity. This result suggests that the influence of negative vorticity on the steepness of free surface elevation is opposite to that of uniform up-flow and vice versa. In addition, the effect of water depth on the steepness can be neglected when $\mu>5$.

Appendix A

The solutions for the first order can be obtained as follows:

$$\phi_{01y}=0,\quad \zeta_{01}=0,$$
$$\phi_{11}=A\frac{\cosh\left[k\left(y+h\right)\right]}{\cosh\left(kh\right)},\quad \zeta_{11}=\frac{\mathrm{i}\omega\left(1+X-\bar{u}\right)}{g}A,$$

where $A(\eta,\tau)$ is the slowly varying amplitude, which is used to represent all other terms. We set

$$c=\frac{\omega}{k},\quad \bar{u}=\frac{U}{c},\quad \mu=kh,$$
$$\sigma=\tanh\mu,\quad \bar{\Omega}=\frac{\Omega}{\omega},\quad X=\sigma\bar{\Omega},$$

where c is the wave velocity, $\bar{u}$ is the dimensionless uniform flow, μ is the dimensionless water depth, and $\bar{\Omega}$ is the dimensionless vorticity. The linear dispersion relation can be derived as

$$\omega^2\left(1+X-\bar{u}\right)\left(1-\bar{u}\right)=gk\sigma.$$

The solutions for the second order can be obtained as follows:

$$\begin{aligned}
\phi_{02y} &= 0,\\
\phi_{12} &= D\frac{\cosh\left[k\left(y+h\right)\right]}{\cosh\left(kh\right)}\\
&\quad -\mathrm{i}A_\eta\frac{\left(y+h\right)\sinh\left[k\left(y+h\right)\right]-h\sigma\cosh\left[k\left(y+h\right)\right]}{\cosh\left(kh\right)},\\
\zeta_{12} &= \frac{1}{g}\left[c_{\mathrm{g}}-c\bar{u}+h\left(1-\sigma^2\right)\Omega\right]A_\eta+\frac{\mathrm{i}\omega\left(1+X-\bar{u}\right)}{g}D,\\
c_{\mathrm{g}} &= \partial\omega/\partial k\\
&= \frac{c}{\sigma}\frac{\mu\left(1-\sigma^2\right)\left(1-\bar{u}\right)^2+\sigma\left(1+X-\bar{u}\right)\left(1-\bar{u}\right)}{2+X-2\bar{u}}+c\bar{u},
\end{aligned}$$

D is the slowly varying function to be determined.

$$\begin{aligned}
\phi_{22} &= \frac{\mathrm{i}\omega\left(1+\sigma^2\right)}{4\sigma^2c^2\left(1-\bar{u}\right)^3}[3\left(1-\sigma^2\right)\left(1-\bar{u}\right)^2\\
&\quad +3X\left(1-\bar{u}\right)+X^2]A^2\frac{\cosh\left[2k\left(y+h\right)\right]}{\cosh\left(2kh\right)},\\
\zeta_{22} &= -\frac{k}{2\sigma c^2\left(1-\bar{u}\right)^4}[\left(3-\sigma^2\right)\left(1-\bar{u}\right)^2\\
&\quad +X\left(3+\sigma^2\right)\left(1-\bar{u}\right)+X^2]A^2.
\end{aligned}$$

The long wave equation of mean flow (ϕ_{01}), which is important in the development of the modulational instability, is obtained for the third order

$$\begin{aligned}
&\left[\left(c_{\mathrm{g}}-c\bar{u}\right)\left(c_{\mathrm{g}}-c\bar{u}+\Omega h\right)-gh\right]\phi_{01\eta}\\
&= [k\omega\left(2+X-2\bar{u}\right)\left(1+X-\bar{u}\right)\left(1-\bar{u}\right)^{-1}\\
&\quad +k^2\left(1-\sigma^2\right)\left(c_{\mathrm{g}}-c\bar{u}\right)]\left|A\right|^2,\\
g\zeta_{02} &= \left(c_{\mathrm{g}}-c\bar{u}+\Omega h\right)\phi_{01\eta}-k^2\left(1-\sigma^2\right)\left|A\right|^2.
\end{aligned}$$

References

[1] Davey A and Stewartson K 1974 *Proc. R. Soc. Lond. A* **338** 101
[2] Turpin F M, Benmoussa C and Mei C C 1983 *J. Fluid Mech.* **132** 1
[3] Djordjevic V D and Redelopp L G 1978 *Z. Angew. Math. Phys.* **29** 950
[4] Peregrine D H 1976 *Adv. Appl. Mech.* **16** 9
[5] Longuet-Higgins M S and Stewart R W 1961 *J. Fluid Mech.* **10** 529
[6] Kantardgi I 1995 *Coast Eng.* **26** 195
[7] Maciver R D, Simons R R and Thomas G P 2006 *J. Geophys. Res.* **111** C03009
[8] Choi W 2009 *Math. Comput. Simul.* **80** 29
[9] Ma Y X, Dong G H, Perlin M, Ma X Z, Wang G and Xu J 2010 *J. Fluid Mech.* **661** 108
[10] Ma Y X, Ma X Z, Perlin M and Dong G H 2013 *Phys. Fluids* **25** 114109
[11] Sedletsky Y V 2005 *Phys. Lett. A* **343** 293
[12] Toffoli A, Waseda T, Houtani H, Cavaleri L, Greaves D and Onorato M 2015 *J. Fluid Mech.* **769** 277
[13] Thomas R, Kharif C and Manna M 2012 *Phys. Fluids* **24** 127102
[14] Smith R 1976 *J. Fluid Mech.* **77** 417
[15] Henderson K L, Peregrine D H and Dold J W 1999 *Wave Motion* **29** 341

[16] Dysthe K B and Trulsen K 1999 *Phys. Scr.* **T82** 48
[17] Ma Y C 1979 *Stud. Appl. Math.* **60** 43
[18] Peregrine D H 1983 *Austral. Math. Soc. Ser. B* **25** 16
[19] Tao Y S, He J S and Porsezian K 2013 *Chin. Phys. B* **22** 074210
[20] Kharif C and Pelinovsky E 2003 *Eur. J. Mech. B Fluids* **22** 603
[21] Liao B, Dong G, Ma Y and Gao J L 2017 *Phys. Rev. E.* **96** 043111
[22] Touboul J, Charl, J, Rey V and Belibassakis K 2016 *Coast. Eng.* **116** 77
[23] Quinn B E, Toledo Y and Shrira V I 2017 *Ocean Modell.* **112** 33
[24] Weng S C and Yu Z W 1985 *Wave Theory Calculation Principle* (Beijing: Sci. Press) Chap 1 p. 31 (in Chinese)
[25] Song S Y, Wang J and Meng J M 2010 *Acta Phys. Sin.* **59** 1123 (in Chinese)
[26] Zhao L C and Ling L M 2016 *J. Opt. Soc. Am. B* **33** 850
[27] Ling L M, Zhao L C, Yang Z Y and Guo B L 2017 *Phys. Rev. E* **96** 022211
[28] Baronio F, Conforti M, Degasperis A, Lombardo S, Onorato M and Wabnitz S 2014 *Phys. Rev. Lett.* **113** 034101
[29] Baronio F, Chen S H, Grelu P, Wabnitz S and Conforti M 2015 *Phys. Rev. A* **91** 033804
[30] Xie T, Shen T, William P, Chen W and Kuang H L 2010 *Chin. Phys. B* **19** 054102
[31] Xie T, Zou G H, William P, Kuang H L and Chen W 2010 *Chin. Phys. B* **19** 059201
[32] Didenkulova I I, Nikolkina I F and Pelinovsky E N 2013 *JETP Lett.* **97** 194